

An orbiter crossing an accretion disc

Ladislav Šubr and Vladimír Karas

Astronomical Institute, Charles University Prague, V Holešovičkách 2, CZ-180 00 Praha, Czech Republic
E-mail: subr@kocour.ms.mff.cuni.cz; vladimir.karas@mff.cuni.cz

Received, 1999; accepted

Abstract. We further investigate the long-term evolution of a trajectory of a stellar-mass orbiter which is gravitationally bound to a massive central body acting by Newtonian force. The orbiter undergoes repetitionary collisions with an accretion disc. We consider eccentric orbits intersecting the disc once or twice per each revolution and we solve the equations for osculating elements. We find the terminal radii of the orbits and time needed to bring the orbit into the disc plane as function of initial parameters, and we show that previous simplified estimates (derived for the case of low eccentricity) remain valid within factor of two. The discussion presented in this paper offers a toy model of the orbital evolution of a satellite which passes through the rarefied gaseous environment of a stationary disc. We demonstrate that the drag on the satellite should be taken into account in calculations of the stellar distribution near the super-massive black hole in galactic centers. On the other hand, it does not impose serious restrictions on the results of gravitational wave experiments, except in the case of discs with rather high surface density.

Key words: Accretion, accretion-discs – Celestial mechanics, stellar dynamics

1. Introduction

Rapid stellar motion in galactic centers reflects properties of a presumed supermassive compact body in the nucleus (Binney & Tremaine 1987; Merrit & Quinlan 1998a, b). One can define the sphere of influence, $r_h = GM/\langle\sigma\rangle^2$, which determines the region of space where gravity of the centre dominates over more remote parts of the galaxy ($M \gtrsim 10^6 M_\odot$ is the central mass, $\sigma \approx 10^2$ km/s is velocity dispersion). Inside r_h , a star can be considered as a satellite orbiting around the central body. We introduce gravitational radius $r_g = 2GM/c^2$, which characterizes

compactness of that body and provides a natural length-scale for the problem discussed in this paper. When expressed in terms of r_h and r_g , we will explore in this paper the region $r_g \ll r \ll r_h$.

Several mechanisms act as perturbations on almost free motion of orbiters in the central gravitational field inside r_h : gravity of the background galaxy, dynamical friction in the field of other orbiters, energy losses due to gravitational radiation, tidal interactions, and friction caused by the rarefied gaseous environment (see Rees 1998 for a recent review). Here we will concentrate on the latter effect, namely, we will consider the long-term evolution of orbital parameters (eccentricity e , semimajor axis a , inclination i , argument of pericentre ω) of the orbiter which crosses the plane of an accretion disc (Fig. 1). We assume that the disc is geometrically thin (collisions will be treated within the impulsive approximation) and neglect all other dissipative effects, ablation of the orbiter, corrections due to general relativity, as well as self-gravity of the disc. Some of these effects were examined quite recently by Vokrouhlický & Karas (1998b), Ivanov et al. (1998), and Zurek et al. (1994). In this context, gradual evolution of the disc surface density was explored by Ivanov et al. (1999). Further citations to older works can be found in Syer et al. (1991), Vokrouhlický & Karas (1993), and Artymowicz (1994).

The impulsive approximation ignores effects of resonances, and it assumes nonzero inclination of the orbit with respect to the disc plane. Our calculations thus do not apply to the case when the orbiter remains embedded inside the disc, the situation which has been widely discussed because of its profound implications for describing the formation of stars and planets (Lin et al. 1999; Bryden et al. 1999). Also, we do not consider possible disruption of the orbiter by the central body; this process has been discussed by many authors, e.g. Kim et al. (1999) very recently. Under these assumptions, the orbital evolution can be solved in two steps: First, parametric relations for osculating elements are obtained which determine the shape of the orbit ($e(i)$, $a(i)$, etc). Next, the temporal depen-

Send offprint requests to: L. Šubr

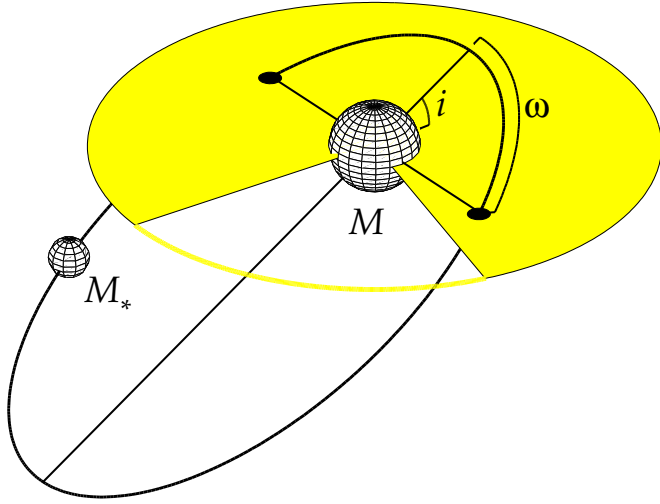


Fig. 1. Geometry of the model. The satellite (mass $M_* \approx M_\odot$) follows a slowly evolving elliptical orbit around more massive central body ($M \approx 10^8 M_\odot$). Argument of pericentre ω and inclination angle i specify orientation of the ellipse. In the present model, action of the disc matter upon the satellite depends only on the disc properties at the places of intersections. For $\omega = \pi/2$ (as in this sketch) both intersections with the disc occur at the same distance, while the case is just opposite for $\omega = 0$ (the places of intersections then correspond to the pericentre and the apocentre, respectively).

dences are examined. Although the present discussion is very much simplified, it captures basic properties of the mechanism driving the orbital evolution, and it offers a toy model which can be used as a test bed for more complicated and astrophysically realistic studies.

In this paper we extend discussion of Vokrouhlický & Karas (1998a; cited as VK hereafter) who studied the orbital evolution under the assumption that orbiter's trajectory intersects the disc only once per revolution. Such an assumption applies to the case when the disc has a finite radial extent and the orbiter follows an eccentric path (the initial stage of the capture from an energetically unbound state). Regarding the description of the disc matter and its mutual interaction with the orbiter, VK adopted several assumptions which are quite plausible for this type of the toy model: a geometrically thin disc rotating at Keplerian velocity in purely azimuthal direction. It was further assumed that the disc itself does not change with time; in particular, dissipative waves induced by the orbiter and the possibility of opening of a gap was not taken into account. These simplifying assumptions are maintained also in the present paper.

Gradual circularization and precession lead eventually to the orbit with two intersections per revolution; at this moment the analytical solution from VK ceases to be valid. Terminal stages of the evolution were treated by Rauch (1995) under approximation of zero and moderate eccentricity, but orbits with large eccentricity could not

be fully examined in terms of an analytic solution, because the two intersections can occur at different radial distances. One thus needs to specify surface density of the disc as a function of radius. We write down corresponding evolutionary equations and solve them numerically under the assumption of the power-law surface density profile. We examine the temporal evolution of orbital parameters, showing that a very special orientation of the trajectory, $\omega = \pi/2$ (when both intersections are at the same r), represents a stable configuration which can be treated analytically. In other words, our present discussion extends previous discussion of the initial period of the orbital evolution, and it concerns also the intermediate stage, when two intersections per revolution have already developed while inclination is still nonzero.

2. Equations for orbital parameters

The basic formulation of the problem follows VK, in particular, the osculating elements of the orbiter are updated at every intersection with an axially symmetric disc, which is described by surface density $\Sigma_d \propto r^s$ ($s = \text{const}$) and by orbital velocity $\mathbf{v}_d = v_\phi \mathbf{e}_\phi$. It appears natural to consider Keplerian rotation of the disc, $v_\phi \equiv v_k = \sqrt{GM/r}$, which fits with the assumption about its small geometrical thickness, and enables us to introduce vertically integrated quantities in the standard manner (we examined also different rotation laws; Karas & Šubr 1999). The central body attracts the orbiter by Newtonian force. Passages through the disc are treated as inelastic collisions which, by assumption, do not affect the properties of the disc and of the orbiter itself. Stated in a different way, disc material located along the orbiter's path transfers part of its momentum to the orbiter, but then the disc restores its original stationary state before the next collision occurs. Collisions thus lead to tiny changes of the orbiter's velocity, $\mathbf{v} \rightarrow \mathbf{v}'$. The momentum conservation law gives

$$\mathbf{v}' = \frac{1}{A+1} \left[v_r \mathbf{e}_r + v_\vartheta \mathbf{e}_\vartheta + (v_\varphi + A v_k) \mathbf{e}_\phi \right], \quad (1)$$

where $A(r) \equiv \Sigma_d v_{\text{rel}} \Sigma_*^{-1} v_\vartheta^{-1}$. Here, v_{rel} is the relative speed of the orbiter and the disc matter, while Σ_* is surface density ascribed to the orbiter and defined by $\Sigma_* = M_* / (\pi R_*^2)$ (quantities denoted by asterisk refer to the orbiter). At every collision, a tiny kick changes velocity according to Eq. (1) and leads to corresponding changes of orbiter's specific (per unit mass) binding energy E , specific angular momentum L , its projection L_z onto rotation axis, and radial velocity component v_r :

$$\delta E = -\frac{1}{2} \delta v^2 = \frac{A}{ay} (2z - y + xz^{3/2}), \quad (2)$$

$$\delta L = r \delta v_t = A \sqrt{\frac{ay}{z}} (x - \sqrt{z}), \quad (3)$$

$$\delta L_z = r \delta v_\varphi = A \sqrt{\frac{ay}{z}} (1 - x\sqrt{z}), \quad (4)$$

$$\delta v_r = A \sqrt{\frac{2z - z^2 - y}{ay}}; \quad (5)$$

here we introduced variables $x = \cos i$, $y = 1 - e^2$, $z = 1 + e \cos \omega$, and we expanded right-hand sides of Eqs. (2)–(5) to the first order in A (since we deal with a small perturbation of the orbit). The collisions occur, in general, twice per each revolution of the orbiter, at the ascending and descending nodes, which will be denoted by subscripts “1” and “2”, respectively. Hydrodynamical drag acts when the orbiter passes across the nodes. By adding the two contributions one obtains

$$da = 2A_1 ay^{-1} \left(y - 2z + xz^{3/2} \right) + 2A_2 ay^{-1} \left(y - 4 + 2z + x(2 - z)^{3/2} \right), \quad (6)$$

$$dx = A_1 \frac{1 - x^2}{\sqrt{z}} + A_2 \frac{1 - x^2}{\sqrt{2 - z}}, \quad (7)$$

$$dy = 2A_1 \left(2z - 2y + \frac{xy}{\sqrt{z}} - xz^{3/2} \right) + 2A_2 \left(4 - 2z - 2y + \frac{xy}{\sqrt{2 - z}} - x(2 - z)^{3/2} \right), \quad (8)$$

$$dz = 2A_1 (x\sqrt{z} - z) + 2A_2 (2 - z - x\sqrt{2 - z}). \quad (9)$$

Eqs. (6)–(9) determine the orbital elements in a parametric form, and we can adopt x as a convenient parameter. Notice that the time dependence has not yet been involved explicitly. Temporal evolution can be examined by introducing the orbital period $dt = 2\pi a^{3/2} / \sqrt{GM}$.

In further equations we take advantage of the fact that the assumed density profile, $\Sigma_d = K (r/r_g)^s \Sigma_*$, enables us relate A 's at two different radii:

$$A_1 = K \frac{(ay)^s}{z^{s+1}} \sqrt{\frac{3z - y - 2xz^{3/2}}{1 - x^2}}, \quad (10)$$

$$A_2 = K \frac{(ay)^s}{(2 - z)^{s+1}} \sqrt{\frac{6 - 3z - y - 2x(2 - z)^{3/2}}{1 - x^2}}. \quad (11)$$

Initially, the orbit is energetically bound or parabolic ($E \geq 0$) with $a = a_0$, $i = i_0$, and $\omega = \omega_0$. Subsequent evolution decreases inclination and eccentricity, and it causes slow precession in ω . Naturally, there is a lower limit on inclination, which determines a moment when integration of our evolutionary equations must be terminated for at least two reasons. First, the nature of the problem becomes different once the orbiter is fully embedded in the disc (Lin et al. 1999; Goldreich & Tremaine 1980). Second, the assumption (1) about impulsive collisions requires the relative speed to be supersonic.

Regarding the latter condition, we can write, for a satellite on a quasi-circular Keplerian orbit, $v_K \approx 2.1 \times 10^{10} (r/r_g)^{-1/2} \text{ cm s}^{-1}$. Therefore, $v_{\text{rel}} \approx 4.2 \times 10^{10} \sin(i/2) (r/r_g)^{-1/2} \text{ cm s}^{-1}$, which is to be compared with the speed of sound v_s . For example, in the standard

Shakura-Sunyaev accretion disc (Frank et al. 1992) with the central mass $M = 10^8 M_\odot$, the accretion rate $\dot{M} = 0.01 \dot{M}_{\text{Edd}}$ (\dot{M}_{Edd} is the accretion rate corresponding to Eddington luminosity), and viscosity parameter $\alpha = 0.1$, one obtains $v_s \approx 1.27 \times 10^7 (r/r_g)^{3/8} \text{ cm s}^{-1}$, and the condition $v_{\text{rel}} \gg v_s$ then reads $\sin(i/2) \gg 3.1 \times 10^{-4} (r/r_g)^{7/8}$.

Inclined orbits can be further distinguished into two sub-cases: Those with (i) a single intersection with the disc plane per revolution, and (ii) two intersections per revolution.

2.1. The initial phase: single intersection

Before describing the results of numerical integration we recall that the parametric analytical solution was given in VK under the assumption that collisions occur only once per revolution, at the inner orbital node (while the more remote node was assumed to lie beyond the outer edge of the disc). This situation corresponds to the initial stage with large eccentricity and appropriate orientation of the ellipse in terms of ω . In this case, one can verify that Eqs. (6)–(9) with $A_2 = 0$ are equivalent to Eqs. (20)–(23) of VK. The corresponding solution reads

$$a = zy^{-1} r_0, \quad (12)$$

$$y = \frac{B_2 (1 - x^2) + x (x + 4B_1 \sqrt{1 - x^2})}{(x + B_1 \sqrt{1 - x^2})^4}, \quad (13)$$

$$z = (B_1 \sqrt{1 - x^2} + x)^{-2}, \quad (14)$$

where r_0 , B_1 , B_2 are constants of integration. We recall that, in Eqs. (12)–(14), x stands as parameter. Time does not enter in mutual relations among $a(x)$, $y(x)$, and $z(x)$. In accordance with the previous definition, x has a physical meaning of cosine of inclination, and one can find its temporal dependence by solving implicit relation

$$t = \frac{1}{K} \int_{x_0}^x z^{3/2}(\bar{x}) \left[\frac{z(\bar{x})}{a(\bar{x})y(\bar{x})} \right]^s (1 - \bar{x}^2)^{-1/2} \times \left[3z(\bar{x}) - y(\bar{x}) - 2\bar{x}z^{3/2}(\bar{x}) \right]^{-1/2} d\bar{x}. \quad (15)$$

2.2. The subsequent phase: two intersections

The orbit eventually develops two intersections per revolution, and one has to resort to a numerical treatment of the problem. However, we checked (see below) for the wide range of starting parameters that the results do not differ substantially from the case with special orientation, $\omega_0 = \pi/2$ (i.e. $z = 1$), which can still be treated analytically. In addition, one can verify that this particular orientation of the orbit is linearly stable, or, in other words, the orbital evolution restores the initial argument of the nodes if slightly perturbed from $\omega = \pi/2$. This conclusion holds for Σ_d decreasing with radius ($s < 0$), but it requires a further remark: It was shown (Vokrouhlický &

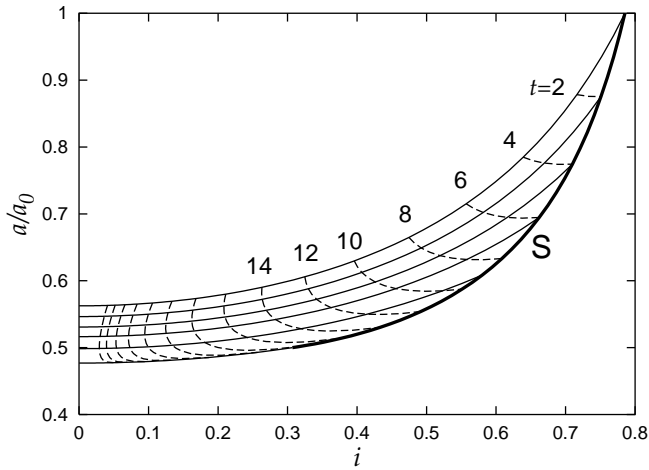


Fig. 2. Semimajor axis a (ordinate, units of a_0) versus inclination i (abscissa). Inclination decreases from its initial value $i_0 = \pi/4$ down to zero, while a decreases from $a = a_0$ to the final $a = a_f$ which depends on position of the outer edge of the disc. First, the evolution follows the thick solid line **S** (single intersection per each orbital revolution), then one of thin solid lines (two intersections per revolution). Dashed curves indicate lines of constant time (arbitrary units). Initial $\omega_0 = 0$, $e_0 = 0.5$. See the text for details.

Karas 1998b) that the claim about the stability is not true when the disc gravity is taken into account. In that case the stability could be maintained only if the orbiter–disc interaction is substantially stronger than it follows from Eq. (1), perhaps due to turbulence or different nature of the collisions. In fact, one should take the disc gravity into account also for self-consistency reasons (although we ignore it here), because both gravitational effects of the disc and its dissipative influence on the passing orbiter arise from the same distribution of matter.

The solution of the $\omega = \pi/2$ case is

$$a = \frac{C_1(1+x)}{(1+x)^3 - C_2(1-x)}, \quad (16)$$

$$y = 1 - C_2 \frac{(1-x)}{(1+x)^3}, \quad (17)$$

$$z = 1, \quad (18)$$

$$t = \frac{1}{K} \int_{x_0}^x \frac{[a(\bar{x})y(\bar{x})]^{-s} d\bar{x}}{\sqrt{(3-y(\bar{x})-2\bar{x})(1-\bar{x}^2)}}, \quad (19)$$

where constants C_1 and C_2 are to be determined from initial values of $x = x_0$ and $y = y_0$.

For $e = 0$ one obtains $C_2 = 0$, and Eqs. (16)–(18) thus reproduce Rauch’s (1995) formula (7) for the final value of semimajor axis of the circular orbit as function of its initial value and initial inclination. In the present notation,

$$a = C_1(1+x)^{-2}. \quad (20)$$

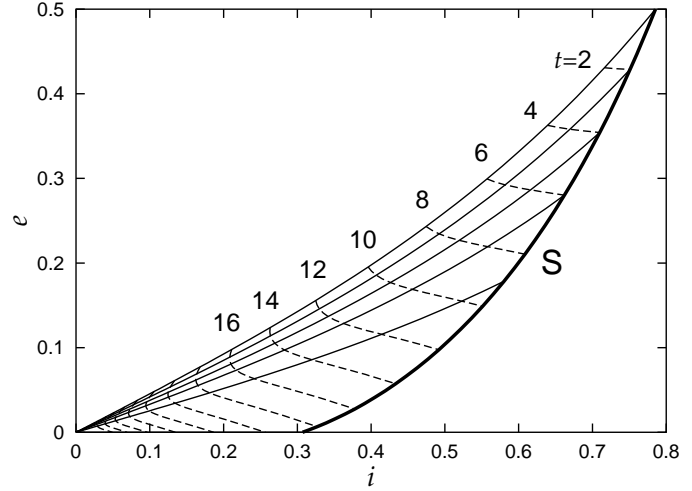


Fig. 3. Eccentricity e versus inclination i for the same initial parameters as in Fig. 2. Here, $i_0 = \pi/4$, $\omega_0 = 0$. Again, the thick solid line shows the initial phase of single intersection, while thin lines correspond to the subsequent period with two intersections.

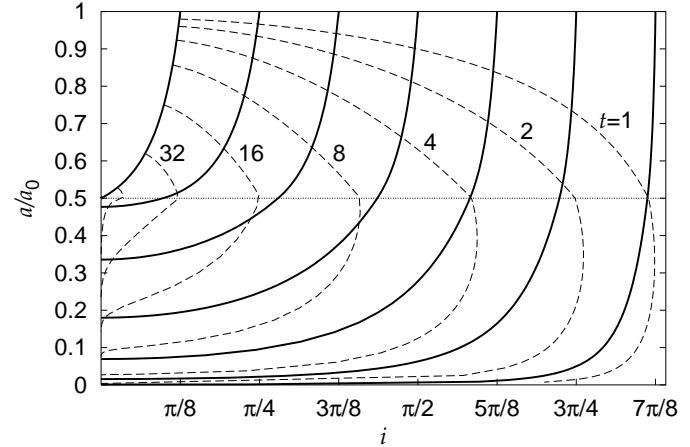


Fig. 4. Semimajor axis a versus inclination i (solid lines) for orbits with different i_0 (initial inclination). Contours of constant time are also shown (dashed; time is given with each curve in arbitrary units). Other parameters as in Fig. 2. Trajectories in this figure start with $a = a_0$, $i = i_0$, and circularize at $a = \frac{1}{2}a_0$. Then they proceed, already with $e = 0$, down to terminal radius a_f at $i = 0$.

Denoting the initial semimajor axis by $a_0 = a(i_0)$, one obtains for the constant

$$C_1 = a_0(1 + \cos i_0)^2 = 4a_0 \cos^4(i_0/2). \quad (21)$$

Temporal evolution (19) can be integrated after specifying the surface density profile by parameter s :

$$t = \pi K^{-1} C_1^{3/2-s} I_{(7-4s)/2}, \quad (22)$$

where $I_\gamma(x) = \int_{x_0}^x (1+\bar{x})^{-\gamma} \sqrt{1-\bar{x}} d\bar{x}$. Integration can be carried out in terms of elementary functions for suitable

values of s (in particular for $s = -3/4$) by applying recurrent formula $2(\gamma-1)I_\gamma = (\gamma-3)I_{\gamma-1} - (1+x)^{1-\gamma}\sqrt{1-x}$ and $I_{1/2} = \arcsin x$. For other values of s , numerical integration is straightforward.

3. Results

We solved Eqs. (6)–(9) with different radial profiles of the surface density and different rotation laws of the disc matter. Numerical analysis provides us with estimates of accuracy of the previous results, which were restricted either by assuming low eccentricity (the final evolutionary stage of the orbit), or, in turn, by ignoring collisions at the orbital node which is farther away from the centre (the initial stage). In other words, we relaxed some assumptions about eccentricity and orientation of the orbiter’s trajectory.

Fig. 2 shows semimajor axis as a function of inclination, $a(i)$. The orbital evolution proceeds from the initial state, $a_0 = a(i_0)$, to the final a_f at $i = 0$ (when orbiter’s orbit plunges into the disc plane). Thick solid line (denoted by “S”) corresponds to the evolutionary stage with the single intersection, which is governed by Eqs. (12)–(14). (We checked that this analytical solution, valid during the phase of single intersections, is reproduced also by the numerical solution which will be used further.) The orbital evolution follows the line S to the point when two intersections occur. The actual moment when this happens is determined by initial orientation of the ellipse and by the radial extent of the disc. Subsequent evolution is disjointed from the thick line, and it goes along one of thin solid lines, which were constructed according to Eqs. (16)–(18). Only this latter part of the solution depends on the value of s (here we set $s = -3/4$, corresponding to the outer region in the standard thin disc model). Dashed lines correspond to $t = \text{const}$ in Eq. (19). They are plotted with constant time steps of $\Delta t = 2$ (arbitrary units) as indicated in the graph. For clarity of the graph, we do not show the lines of constant time near $i = 0$ because evolution of the system slows down visibly when inclination is small. Notice that the final radius of inclined orbits ranges between $0.48 \leq a_f/a_0 \leq 0.57$, lower values corresponding to the case when the branches with two intersections develop late in the course of evolution. One can conclude that even if the moment when two intersections per revolution occur was unknown (e.g. because location of the outer disc edge is left unspecified), still the final radius could be estimated with the relative error less than about 0.15. In this plot we choose $\omega_0 = 0$, because such initial orientation of the ellipse captures a long period of evolution when the ellipse has a single intersection per revolution. We recall that for $\omega = 0$ the intersection is at the pericentre, while the other passage across the disc plane occurs at the apocentre; cf. Fig. 1.

Fig. 3 is constructed in analogous way as Fig. 2, showing eccentricity e as function of i . All the curves of $e(i)$

eventually meet together at the origin, which corresponds to circular orbits of zero inclination (but different a_f ’s). We constructed similar graphs as those in Figs. 2–3 but for different starting parameters, including the counter-rotating orbits; the results of such analysis are qualitatively the same and can be quantified by a_f . Complementary to Fig. 2, Fig. 4 shows $a(i)$ for different i_0 . Again, for the sake of definiteness, the initial ellipse has $e_0 = 0.5$, $\omega_0 = 0$, and the initial pericentre is identified with the outer edge of the disc (i.e. radius above which the disc density is considered as negligible). Such orientation of the orbit could be called as fiducial in our examples concerning with the capture of a satellite from a remote eccentric trajectory, initially extending well above r_h . All the orbits in this example have a single intersection, which is located exactly at the outer disc edge until a decreases down to half of its initial value, $a = \frac{1}{2}a_0$ (denoted by the horizontal dotted line). At this point the second intersection occurs for the first time.

Terminal radius a_f of a general orbit, with either one or two intersections per revolution, follows from the numerical solution, as it was described in previous paragraphs. Eqs. (16)–(17) represent a good approximation to the numerical solution of Eqs. (12)–(14), which becomes exact for $\omega_0 = \pi/2$. With this orientation of the trajectory we recover the above-quoted formula, originally derived for moderate eccentricity (Rauch 1995): $a_f \approx \frac{1}{4}a_0(1 - e_0^2)(1 + \cos i_0)^2$. A simple formula has obvious practical advantages, and one thus wants to quantify its accuracy. We define the relative error as

$$\Delta a_f(e_0, i_0, \omega_0) \equiv \frac{a_f(a_0, e_0, i_0, \omega_0) - a_f(a_0, e_0, i_0, \pi/2)}{a_0} \quad (23)$$

and show the surface plot of Δa_f in Fig. 5 for $i_0 = 5^\circ$, $s = -3/4$, and different starting ω_0 , e_0 . It is evident from the plot that the difference is substantially reduced when $\omega_0 \rightarrow \pi/2$ and/or $e_0 \rightarrow 0$. Although this plot was constructed for the particular value of i_0 , it turns out that the difference is also reduced for higher initial inclination.

Our discussion is completed by calculating temporal dependences. Time evolution of semimajor axis is shown in Figs. 6–7 for the disc with $\Sigma_d \propto r^{-3/4}$. Here we choose $\omega_0 = \pi/2$, so that the orbit has two branches from the very beginning. Temporal dependences can be computed by direct evaluation of Eq. (19), or Eq. (22) when it applies, but purely numerical integration of original Eqs. (6)–(9) gives the same results. Characteristic time-scale τ (in terms of orbital periods) is determined by ratio of surface densities, $\tau = \Sigma_*/\Sigma_d$. When scaled to the form appropriate for the gas-dominated region of the Shakura-Sunyaev disc around a supermassive compact core (Frank et al. 1992),

$$\Sigma_d = 10^{-4} \left(\frac{\alpha}{0.1} \right)^{-4/5} \left(\frac{\dot{M}}{M_\odot/\text{yr}} \right)^{7/10}$$

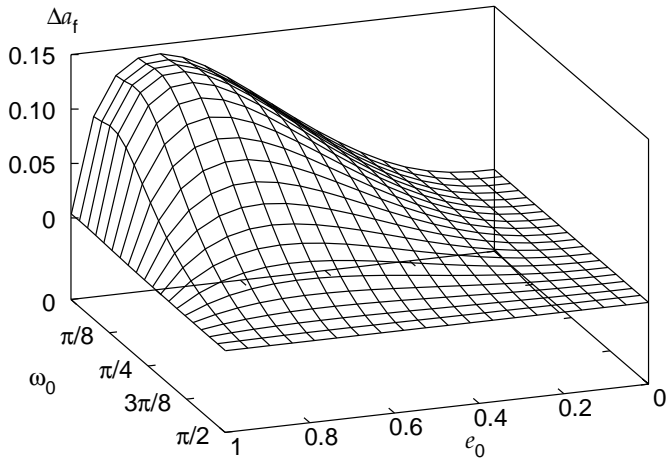


Fig. 5. Relative difference $\Delta a_f(e_0, \omega_0)$ of final radius, as defined in Eq. (23). This figure illustrates the fact that Eqs. (16)–(19) estimate the correct value of a_f with accuracy better than 15% in the whole range of eccentricity.

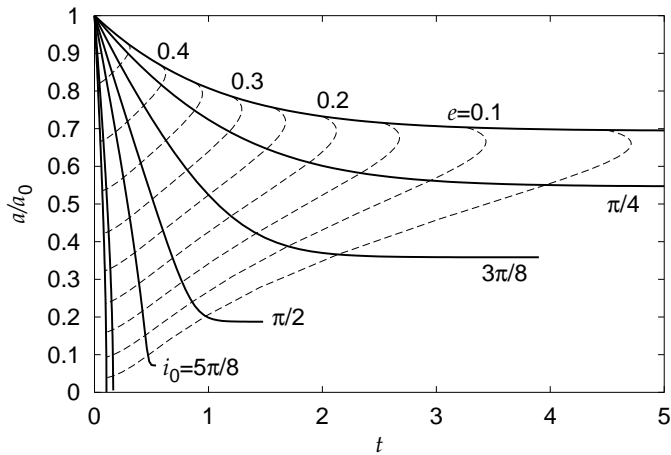


Fig. 6. Time evolution of semimajor axis $a(t)/a_0$ (solid lines). Initial inclination is given with each curve. Isolines of constant eccentricity (dashed) indicate how the pace of orbital evolution eventually slows down in the case of orbits which are almost circular and have small inclination. Again, time is in arbitrary units which can be scaled with the disc surface density (see the text); $e_0 = 0.5$, $\omega_0 = \pi/2$.

$$\times \left(\frac{M}{10^8 M_\odot} \right)^{-1/2} \left(\frac{r}{r_g} \right)^{-3/4} \left[\frac{M_\odot}{r_\odot^2} \right]. \quad (24)$$

From here, the fiducial value of τ corresponding to a solar-size satellite ($\Sigma_* \approx M_\odot/r_\odot^2$) passing across the inner part of disc (where density has maximum) is of the order 10^4 revolutions (inverse of the numerical factor in front of rhs. of Eq. (24)). Scaling with the model parameters is also evident: e.g. for an orbiter at $r \approx 10^4 r_g$, and the disc with viscosity parameter $\alpha \approx 10^{-3}$, accretion rate $\dot{M} \approx 1 M_\odot$ per year, $\Sigma_* = \Sigma_\odot$, one obtains $\tau \approx 10^6$ revolutions, corresponding to $\approx 10^8$ yrs. Although the precise time-scale can

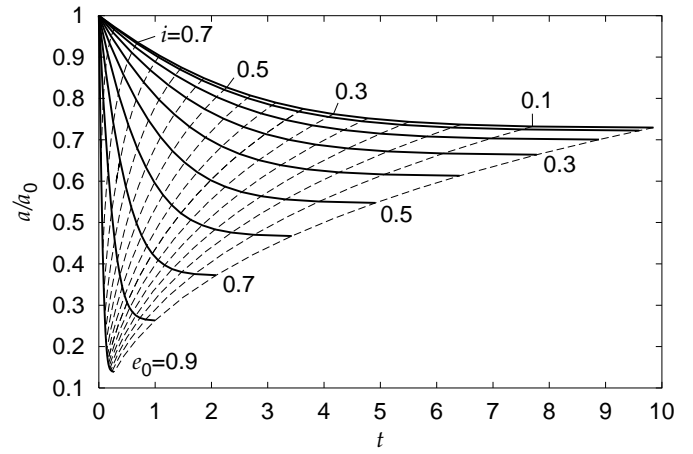


Fig. 7. Time evolution of semimajor axis as in Fig. 6 but for $i_0 = \pi/4$ and different initial eccentricities (solid lines; e_0 is given with each curve). Isolines of constant inclination are shown with constant step 0.05 (dashed).

be computed in a straightforward manner from Eq. (19) above, assuming the disc model, one should be cautious about interpretation of time intervals in physical units. In a realistic model, major uncertainty affecting the constant of proportionality K is connected with poorly known effects of turbulence (Zurek et al. 1996), which tend to enhance the drag on the orbiter. We recall that K stands only in front of the time integral, and it determines temporal dependences in absolute units, but it does not appear in mutual relations among orbital parameters. Knowledge of K is thus unnecessary for determination of the shape of the orbit and its evolution in arbitrary units of time, provided that collisions can be treated as small perturbation.

In the above-given discussion we restricted ourselves to Keplerian discs. This turns out to be rather important assumption because non-Keplerian discs can transfer energy to the orbiter. In such a case, $a(t)$ passes through a minimum at some point and starts increasing again. For example, such behaviour occurs in a disc with constant angular momentum density l (Karas & Šubr 1999), if one can still retain other assumptions of our model, namely the impulsive approximation for collisions ($l = \text{const}$ appears in discussion of discs which acquire substantial geometrical thickness, so that vertically integrated quantities may be too inaccurate).

4. Conclusions

There are two areas where the models, like the one which we discussed here, are relevant. First, the calculations of the stellar distribution in galactic cores (Bahcall & Wolf 1976; Quinlan et al. 1995) predict the presence of density cusps and corresponding integrated-light profiles around the massive black hole. Stellar orbits and, consequently,

the overall form of the cusps will be modified by the presence of gaseous environment. We demonstrated that evolutionary time-scales are typically 1–2 orders of magnitude less than the stellar life time, and the influence of the disc should be thus accounted. This is true especially for active galactic nuclei with enhanced accretion rates, while in the center of Milky Way the gaseous environment is too rarefied to exert any substantial hydrodynamical drag on stars. The smallest resolved scales ($\approx 0.1''$) do not allow direct observational comparisons at present, but this may be possible when better resolution is available (although the direct tracking of individual stars does not seem possible in near future; Kormendy & Richstone 1995).

Another possible application concerns the predicted gravitational waveform patterns from inspiralling satellites. It was suggested (Chakrabarti 1996) that the wave emission may be significantly altered if the satellite moves inside a super-Eddington ($\dot{M} \approx 10^3 \dot{M}_{\text{Edd}}$) flow and passes through shocks there. This could be an interesting possibility but it represents rather exceptional situation. When most of the motion takes place outside the disc, as in our case, the time-scales of the orbital evolution due to the presence of the disc are always much longer than the orbital period, even for quite high accretion rates ($\dot{M} \approx \dot{M}_{\text{Edd}}$), and the production of gravitational waves is virtually unaffected. One should however notice that gaseous environment helps to capture the satellite and bring it down to the low orbit with small inclination, the situation which is needed for the efficient wave emission.

We solved Eqs. (6)–(9), which determine the orbital evolution of a body on an eccentric trajectory evolving adiabatically due to dissipative collisions with the disc. In the general case it is quite obvious from the form of these equations that one has to resort to the numerical approach, but we checked with discs obeying reasonable power-law surface density profiles ($-1 \leq s \leq -0.5$) and Keplerian rotation law that evolution of the true trajectory is well approximated by the corresponding orbit with $\omega_0 = \pi/2$. This case can be integrated analytically [Eqs. (16)–(19)]. Approximate terminal radii of circularized orbits agree with those obtained by numerical integration within precision better than 15%. This conclusion can be put in other words, namely, effects of the disc self-gravity, of different rotation laws, and of mutual collisions among orbiters seem to influence the evolution more substantially than do exact properties of the disc material.

Compared with previous papers, our present discussion has been more general on the level of semi-analytical treatment of the orbits with arbitrary orientation, for which either one or two intersections develop in the course of evolution. In particular we examined how the power-law index of the disc surface-density profile enters in equations for the orbital shape and time evolution of the parameters. It should be quite obvious that we picked up one aspect of a complex problem of the long-term orbital evolution, which will be build into a mosaic to form the complete

picture in astrophysically more realistic models. Various compelling processes were already considered separately. Now we need to take them jointly into account, especially the effects of resonances between the satellite and the disc matter, corrections due to general relativity (of the gravitational field of the central object and energy losses of the orbiter), tidal effects, and gravitational interaction with other satellites. This will certainly require mostly numerical approaches for which analytical estimates of individual processes and toy models, like the present one, provide useful guidelines.

Acknowledgements. We are grateful to the referee for suggestions which helped us to improve the original version of our paper. We also thank D. Vokrouhlický for clarifying discussions and we acknowledge support from the grants GACR 205/97/1165 and 202/99/0261. V.K. thanks for hospitality of the International School for Advanced Studies in Trieste.

References

- Artymowicz P., 1994, ApJ 423, 581
 Bahcall J. N., Wolf R. A., 1976, ApJ 209, 214
 Binney J., Tremaine S., 1987, Galactic Dynamics (Princeton University Press, Princeton)
 Bryden G., Chen Xingming, Lin D. N. C., Nelson R. P., Papaloizou J. C. B., 1999, ApJ 514, 344
 Chakrabarti S. K., 1996, Phys. Rev. D 53, 2901
 Frank J., King A. R., Raine D. J., 1992, Accretion Power in Astrophysics (Cambridge University Press, Cambridge)
 Goldreich P., Tremaine S., 1980, ApJ 241, 425
 Ivanov P. B., Igumenshchev I. V., Novikov I. D., 1998, ApJ 507, 131
 Ivanov P. B., Papaloizou J. C. B., Polnarev A. G., 1999, MNRAS 307, 79
 Karas V., Šubr L., 1999, Proceedings of the 19th Texas Symposium on Relativistic Astrophysics and Cosmology (Paris, 1998), CD version, in preparation
 Kim S. S., Park M.-C., Lee H. M., 1999, ApJ 519, 647
 Kormendy J., Richstone D., 1995, ARA&A 33, 581
 Lin D. N. C., Papaloizou J. C. B., Bryden G., Ida S., Terquem C., 1999, in Protostars and Planets IV, eds. A. Boss, V. Mannings & S. Russell, in press
 Merrit D., Quinlan G. D., 1998a, ApJ 498, 625
 Merrit D., Quinlan G. D., 1998b, ApJ 509, 933
 Quinlan G. D., Hernquist L., Sigurdsson S., 1995, ApJ 440, 554
 Rauch K. P., 1995, MNRAS 275, 628
 Rees M. J., 1998, in Black Holes and Relativistic Stars, ed. R. M. Wald (University of Chicago Press, Chicago), chapt. 4
 Syer D., Clarke C. J., Rees M. J., 1991, MNRAS 250, 505
 Vokrouhlický D., Karas V., 1993, MNRAS 265, 365
 Vokrouhlický D., Karas V., 1998a, MNRAS 293, L1 (VK)
 Vokrouhlický D., Karas V., 1998b, MNRAS 298, 53
 Zurek W. H., Siemiginowska A., Colgate S. A., 1994, ApJ 434, 46
 Zurek W. H., Siemiginowska A., Colgate S. A., 1996, ApJ 470, 652

This article was processed by the author using Springer-Verlag L^AT_EX A&A style file L-AA version 3.